Quantum optimal control theory for the shaping of flying qubits

Xue Dong,[1] Xi Cao,[1] Wen-Long Li,[1] Guofeng Zhang,[2,3,4,*] Zhihui Peng,[5,6,†] and Re-Bing Wu[1,‡]

[1] *Center for Intelligent and Networked Systems, Department of Automation, Tsinghua University, Beijing 100084, China*

[2] *Department of Applied Mathematics, The Hong Kong Polytechnic University, Hung Hom, Kowloon, Hong Kong, China*

[3] *The Hong Kong Polytechnic University Shenzhen Research Institute, Shenzhen, Guang Dong 518057, China*

[4] *Research Institute for Quantum Technology, The Hong Kong Polytechnic University, Hong Kong, China*

[5] *Key Laboratory of Low-Dimensional Quantum Structures and Quantum Control of Ministry of Education, Department of Physics and Synergetic Innovation Center of Quantum Effects and Applications, Hunan Normal University, Changsha, China*

[6] *Hefei National Laboratory, Hefei, China*

(Received 20 April 2024; revised 5 November 2024; accepted 8 January 2025; published 21 April 2025)

The control of flying qubits carried by itinerant photons is ubiquitous in quantum networks. In addition to their logical states, the shapes of flying qubits must also be tailored for high-efficiency information transmission. In this paper, we introduce quantum optimal control theory to the shaping of flying qubits. Building on the flying-qubit control model established in our previous work, we design objective functionals for the generation of shaped flying qubits under practical constraints on the emitters and couplers. Numerical simulations employing gradient-descent algorithms demonstrate that the optimized control can effectively mitigate unwanted level and photon leakage caused by these nonidealities. Notably, while coherent control offers limited shaping capacity with a fixed coupler, it can significantly enhance the shaping performance when combined with a tunable coupler that has restricted tunability. The proposed optimal control framework provides a systematic approach to achieving high-quality control of flying qubits using realistic quantum devices.

DOI: 10.1103/PhysRevApplied.23.044045

I. INTRODUCTION

The rapid development of quantum information processing technologies has attracted extensive attention from academia and industry [1]. In the near future, quantum information processing units will be interconnected for secure communication and distributed quantum computing [2]. Central to this vision, the efficient control of flying qubits is vital for high-fidelity quantum information transmission over quantum networks [3,4].

Flying qubits can be physically carried by itinerant photonic fields [5,6], acoustic waves [7], or electrons [8], with photonic flying qubits being the most widely used in practice. Depending on the wavelength, photonic flying qubits may work in the optical regime when being used for long-distance communication [9]. They can also be generated and manipulated in the microwave regime for interconnection with solid-state quantum information processing devices [10]. In this paper, we are mainly concerned with microwave flying qubits, for which superconducting quantum systems are excellent candidates for emitters and receivers due to their frequency tunability, long coherence time, and field confinement to one-dimensional transmission lines without additional spatial pattern matching [11].

From the viewpoint of quantum input-output theory, flying qubits can be treated as the quantum input of a receiver or quantum output of an emitter. Existing studies have shown that flying qubits sent from an emitter must be well shaped to match to the receiver for complete absorption [12–14]. This gives rise to the flying-qubit shaping problem to be studied in this paper.

In most flying-qubit generation systems, the emitter is coupled to the waveguide through an intermediate cavity to enhance emitter-photon interaction. This cavity also facilitates shaping control by enabling variation of its instantaneous photon emission rate [15,16] or modulation of the effective emitter-cavity coupling induced by a coherent driving field on the cavity [10,12]; however, cavities inherently limit the transmission bandwidth of flying qubits and require strict frequency alignment. Moreover, they may also cause the random release of unwanted photons.

*Contact author: guofeng.zhang@polyu.edu.hk
†Contact author: zhihui.peng@hunnu.edu.cn
‡Contact author: rbwu@tsinghua.edu.cn

Regarding these issues, cavity-free systems using tunable emitters and couplers [13,17–20] offer a more efficient approach [21,22]. Theoretical studies indicate that flying qubits can be shaped arbitrarily using an ideal two-level emitter and an ideal tunable coupler [23–25], and this has been experimentally demonstrated in various experiments in superconducting systems [20,26,27].

Nonetheless, realistic emitters and couplers are inherently nonideal. In superconducting systems, transmon qubits are frequently used due to their long lifetime; however, they cannot be regarded as true two-level systems because of their weak anharmonicity. This limitation can result in significant control errors caused by level leakage [22]. Additionally, regarding the emitter, a very strong coupling beyond the tunable range may be required when the desired photon shape has a sharply rising part. For example, exponentially rising flying qubits are often preferred in practice because they can be fully captured by the receiver without the need for a tunable coupler [24], but generating such flying qubits would require infinitely strong coupling, which is unattainable with existing couplers [13,28–31].

As a result, additional controls must be implemented when the coupler fails to provide sufficient tunability. It seems that the only option available is the coherent driving field, which is typically employed to prepare the emitter's state; however, this is generally avoided for shaping due to the undesirable multiphoton emissions it produces. Nevertheless, we will demonstrate in this paper that coherent control can be designed to improve shaping performance using quantum optimal control theory, which has been proven highly effective in the manipulation of stationary qubits [32–34]. To the best of our knowledge, no such investigations exist in the literature except in linear quantum systems [35].

The remainder of this paper is organized as follows. Section II introduces the mathematical model of the flying-qubit control system implemented by a transmon-qubit emitter. Based on this model, the objective functionals for three associated flying-qubit control tasks are introduced in Sec. III. In Sec. IV, the gradient-descent algorithm applied to the proposed objective functionals is numerically tested. Finally, conclusions are drawn in Sec.V.

II. THE MODELING OF FLYING-QUBIT GENERATION SYSTEMS

To illustrate how optimal control theory can effectively address various nonidealities in the flying-qubit shaping system, we assume that the emitter is a superconducting transmon qubit that cannot be treated as a perfect two-level system. The design methodology can also be readily adapted to other types of emitters.

As shown in Fig. 1, the transmon-qubit emitter is inductively connected to a unidirectional waveguide (transmission line) via a gmon coupler, the coupling strength of

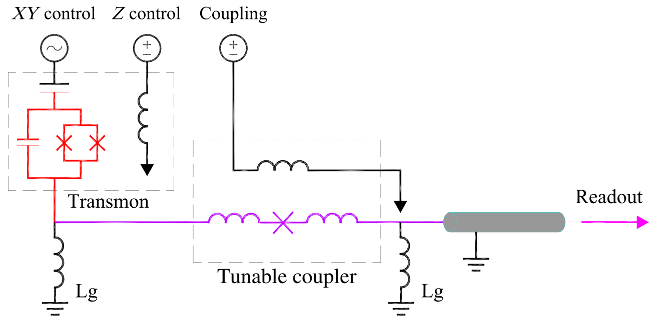

FIG. 1. Schematic of a microwave flying-qubit emitter implemented by a transmon qubit. The emitter is inductively coupled to a transmission-line waveguide through a tunable gmon coupler. The transmon qubit is frequency tunable by the Z control, and its state can be coherently manipulated by the XY microwave driving field.

which can be altered in real time [20,28]. The frequency of the transmon-qubit emitter is tuned by the Z-control line, and its state transition can be manipulated by the XY microwave driving field.

Let $|\text{vac}\rangle$ be the vacuum state of the photon field in the waveguide and $\hat{b}(t)$ be its temporal annihilation operator, which satisfies the singular commutation relation $[\hat{b}(t), \hat{b}^\dagger(t')] = \delta(t-t')$ [35,36]. In this work, we are concerned with the generation of shaped flying qubits, and the waveguide can thus be assumed to be empty when $t<0$. A pulsed single-photon state is defined as follows:

$$|1_\xi\rangle = \int_0^\infty \xi(t)\hat{b}^\dagger(t)\,\mathrm{d}t|\text{vac}\rangle, \tag{1}$$

in which the complex-valued function $\xi(t)$ represents the temporal shape of the single-photon pulse. The normalization property of $|1_\xi\rangle$ requires that the shape function $\xi(t)$ satisfies

$$\int_0^\infty |\xi(t)|^2\,\mathrm{d}t = 1. \tag{2}$$

Herein, we assume that the emitter is coupled to the waveguide with 100% efficiency, meaning that the emitted photons all enter the waveguide. A straightforward two-stage protocol for generating flying qubits is to first drive the transmon qubit to some desired superposition state, say $c_0|0\rangle + c_1|1\rangle$, and then transfer it to the photon field state $c_0|\text{vac}\rangle + c_1|1_\xi\rangle$ via spontaneous emission. The single-photon shape $\xi(t)$ is determined by the real-time tuning of the coupler. Here, the vacuum state $|\text{vac}\rangle$ and the single-photon state $|1_\xi\rangle$ represent the logical states 0 and 1, respectively, of the flying qubit. Thus, to fully characterize the flying-qubit state, it is essential not only to identify the logical state but also to incorporate the shape function.

Under general circumstances, the photon field may also involve multiphoton components due to imperfect state preparation or the presence of a coherent driving field. The corresponding flying-qubit state can be expressed in the following form:

$$|\Xi\rangle = \xi^{(0)}|\mathrm{vac}\rangle + \int_0^\infty \xi^{(1)}(t)b^\dagger(t)\,\mathrm{d}t|\mathrm{vac}\rangle + |\Xi'\rangle, \quad (3)$$

where $\xi^{(0)}$ is the probability amplitude of the vacuum state, $\xi^{(1)}(t)$ is the shape of the single-photon component, and $|\Xi'\rangle$ represents the remaining multiphoton components. Because the full state $|\Xi\rangle$ is always normalized, we have

$$\left|\xi^{(0)}\right|^2 + \int_0^\infty \left|\xi^{(1)}(t)\right|^2 \,\mathrm{d}t \le 1. \quad (4)$$

In the literature, the few-photon emission process induced by time-variant controls (including coherent driving and incoherent tunable coupling) has been studied using scattering theory [37,38] or quantum input-output theory based on quantum stochastic differential equations (QSDEs) [14]. The developed mathematical models enable the calculation of the flying-qubit state as well as the errors induced by multiphoton emission. Here, we leverage the model developed in our previous work [14], which is governed the following nonunitary Schrodinger equation:

$$\dot{V}(t) = -iH_{\mathrm{eff}}(t)V(t), \quad V(0) = \mathbb{I}, \quad (5)$$

where $V(t)$ is the nonunitary evolution operator and

$$H_{\mathrm{eff}}(t) = \frac{\eta}{2}\hat{a}^{\dagger 2}\hat{a}^2 + u(t)\hat{a}^\dagger + u^*(t)\hat{a} - \frac{i\gamma(t)\hat{a}^\dagger\hat{a}}{2} \quad (6)$$

is the effective Hamiltonian. Here, the transmon qubit is treated as an anharmonic oscillator, where $\hat{a}$ is the annihilation operator and η is the anharmonicity. The time-variant function $\gamma(t)$ represents the tunable coupling strength produced by the coupler to the waveguide. The coherent driving field $u(t) = u_x(t) + iu_y(t)$ includes the in-phase and phase-quadrature components $u_x(t)$ and $u_y(t)$.

The flying-qubit state is determined by vacuum and single-photon components, $\xi^{(0)}$ and $\xi^{(1)}(t)$, in Eq. (3). Suppose that the emitter is initially prepared in state $|\psi_0\rangle$ and the coherent control $u(t)$, if present, persists for at most a finite duration. In this case, the emitter eventually decays to its ground state $|0\rangle$ after the flying qubit is released. The flying-qubit state can be calculated as follows [14]:

$$\xi^{(0)} = \langle 0|G(\infty, 0)|\psi_0\rangle, \quad (7)$$

$$\xi^{(1)}(t) = \sqrt{\gamma(t)}\langle 0|G(\infty, t)\hat{a}G(t, 0)|\psi_0\rangle, \quad (8)$$

where

$$G(t, t') = V(t)V^{-1}(t') \quad (9)$$

is the propagator of Eq. (5) from time t' to time t. The intervention of $\hat{a}$ in Eq. (8) indicates the occurrence of a quantum jump at time t that dumps the qubit to its lower-level state and releases a photon into the waveguide.

As a special case, the single-photon component has the following analytic form [14]:

$$\xi(t) = \sqrt{\gamma(t)}\exp\left[-\frac{1}{2}\int_0^t \gamma(\tau)\,\mathrm{d}\tau\right] \quad (10)$$

when $u(t) = 0$ and the initial state is $|\psi_0\rangle = |1\rangle$, which is fully dependent on the tunable coupling $\gamma(t)$. In general cases when $u(t) \neq 0$, the single-photon component has to be numerically calculated.

Note that the multiphoton components $|\Xi'\rangle$ in Eq. (3), which contribute to control errors, need not be explicitly calculated in the optimal control design. This is because the optimization aims to maximize the proportions of vacuum and single-photon components, which naturally leads to the minimization of the unwanted multiphoton components, given that the full state $|\Xi\rangle$ is always normalized.

III. OPTIMAL CONTROL THEORY FOR THE SHAPING OF FLYING QUBITS

The above model indicates that the logical state and the photon shape of the flying qubits can be altered by the tunable coupling $\gamma(t)$ or the driving field $u(t) = u_x(t) + iu_y(t)$, which play the role of incoherent or coherent controls in the flying-qubit shaping. As will be seen later, they can be jointly applied and optimized to improve the shaping performance with nonideal emitters and tunable couplers.

In this section, we will discuss how to formulate the optimal control problems for the generation of shaped flying qubits.

A. Preparation of the standing qubit state

Consider the state preparation of the emitter's state that is to be transferred to the flying qubit. Assume that the emitter is initialized at $|\psi_0\rangle = |0\rangle$ and the target state is $|\psi_P\rangle$, and the coupler is nonideal in that it cannot be completely turned off.

Let $\gamma(t) = \gamma_0 \neq 0$ be the residual coupling strength, and the coherent control function $u(t)$ is to be optimized to minimize the state-preparation error. We present two alternative objective functionals.

The first objective functional is defined as the state-preparation error of the transmon qubit

$$J_1^{\mathrm{ME}}[u(t)] = 1 - \langle\psi_P|\rho(T_0)|\psi_P\rangle, \quad (11)$$

where T_0 is the duration of the control pulse, and the density matrix $\rho(t)$ obeys the following master equation

(ME):

$$\dot{\rho}(t) = -i\left[\frac{\eta}{2}\hat{a}^{\dagger 2}\hat{a}^2 + u(t)\hat{a}^\dagger + u^*(t)\hat{a}, \rho(t)\right] + \gamma_0\left[\hat{a}\rho(t)\hat{a}^\dagger - \frac{1}{2}\rho(t)\hat{a}^\dagger\hat{a} - \frac{1}{2}\hat{a}^\dagger\hat{a}\rho(t)\right]. \quad (12)$$

The master equation can be derived by averaging over the flying-qubit state with the waveguide being taken as a Markovian environment [39,40]. The goal is to maximize the overlap between the emitter state and the target state, thereby minimizing the leakage to higher noncomputational states.

The second objective functional is defined as the control error resulting from photon leakage, because the accompanying decay of excited states alters the population of the computational states. The photon leakage is quantified by the probability of detecting photons in the waveguide before the emitter is steered to the target state $|\psi_P\rangle$:

$$J_1^{\mathrm{QSDE}}[u(t)] = 1 - |\langle\psi_P|G(T_0, 0)|0\rangle|^2, \quad (13)$$

where $G(T_0, 0) = V(T_0)$ can be obtained from Eq. (5). The superscript QSDE refers to "quantum stochastic differential equation" [14], which was used to derive Eq. (5).

B. Direct generation of shaped flying qubits

Suppose that the emitter has been prepared at the target state. With an ideal coupler, the follow-up release of shaped flying qubits can be achieved with the following tuning scheme:

$$\gamma(t) = \frac{|\xi_0(t)|^2}{\int_t^\infty |\xi_0(\tau)|^2\,\mathrm{d}\tau}, \quad (14)$$

where $\xi_0(t)$ is the target shape of the single-photon component. This formula can be derived from Eq. (10).

We now consider the scenario where the coupler cannot be completely turned off or arbitrarily strengthened. In this context, we can introduce $u(t)$ as an auxiliary control alongside $\gamma(t)$, unifying the two-stage flying-qubit generation protocol into a single optimal control task. The corresponding objective functional is defined as the distance between the generated and target flying-qubit states:

$$J_2[u(t), \gamma(t)] = |\xi^{(0)} - c_0|^2 + \int_0^\infty |\xi^{(1)}(t) - c_1\xi_0(t)|^2\,\mathrm{d}t, \quad (15)$$

in which the vacuum and single-photon components of the emitted photon field are

$$\xi^{(0)} = \langle 0|G(\infty, 0)|0\rangle, \quad (16)$$

$$\xi^{(1)}(t) = \sqrt{\gamma(t)}\langle 0|G(\infty, t)\hat{a}G(t, 0)|0\rangle. \quad (17)$$

Note that we adopt the Euclidean distance here for optimization. In practice, one can alternatively use other distance measures.

C. State transfer from the standing qubit to a shaped flying qubit

Consider the control scenario where the emitter has been prepared in some unknown state $|\psi\rangle = c_0|0\rangle + c_1|1\rangle$, and we wish to design a control protocol that transfers the emitter to the flying-qubit state $c_0|\mathrm{vac}\rangle + c_1|1_{\xi_0}\rangle$. The control protocol should be independent of specific values of c_0 and c_1.

The state transfer effectively forms a SWAP gate operation between the emitter and the flying qubit, which can be decomposed into two separate control tasks: (1) the flying qubit should be in the vacuum state when the emitter is initially prepared in state $|0\rangle$; and (2) the flying qubit should be in the single-photon state $|1_{\xi_0}\rangle$ when the emitter is initially prepared in state $|1\rangle$. The sum of the corresponding distances between the generated and target flying-qubit states form the following objective functional:

$$J_3[u(t), \gamma(t)] = \left|1 - \xi^{(0)}\right|^2 + \int_0^\infty |\xi^{(1)}(t) - \xi_0(t)|^2\,\mathrm{d}t, \quad (18)$$

where

$$\xi^{(0)} = \langle 0|G(\infty, 0)|0\rangle, \quad (19)$$

$$\xi^{(1)}(t) = \sqrt{\gamma(t)}\langle 0|G(\infty, t)\hat{a}G(t, 0)|1\rangle. \quad (20)$$

Note that the calculation of the single-photon component Eq. (19) is different from that in Eq. (16), in that it is conditioned on the emitter's initial state $|1\rangle$.

IV. SIMULATION RESULTS

In this section, we detail numerical simulations to test the effectiveness of optimal control in flying-qubit shaping problems. We adopt the L-BFGS quasi-Newton algorithm [41] for the optimization subject to the objective functionals proposed in Sec. III, and the calculation of the corresponding gradient vectors can be found in Appendix A.

Considering practical constraints, we impose that the control pulse $u(t)$ is zero at both the initial and final time instances (i.e., $u(0) = u(T) = 0$). To ensure smoothness during the optimization, we apply a low-pass filter to $u(t)$. Additionally, the control $u(t)$ is constrained with a bound $B = 2\pi \times 80$ MHz. A detailed discussion on how these constraints are managed in the optimization algorithm can be found in Appendix A.

In the simulation, the anharmonicity of the transmon-qubit emitter is set to $\eta = -2\pi \times 200$ MHz, and we retain the first five levels in the model (5) to assess the effect of level leakage. The target shapes of flying qubits considered in the simulations are among the following three types:

(1) exponentially decaying: $\xi_0(t) = \sqrt{\alpha}e^{-\alpha t/2}$;
(2) exponentially rising: $\xi_0(t) = \sqrt{\alpha}e^{\alpha(t-T)/2}$;
(3) symmetrical: $\xi_0(t) = \sqrt{\alpha}\text{sech}(\alpha t/2)$.

Here, α determines the width of the shape function. All the shaped functions are defined on a sufficiently large time interval $[0, T]$.

A. Flying-qubit control under fixed coupling and tunable coherent control

We first investigate the capability of coherent control $u(t)$ on the shaping of flying qubits with a fixed coupler.

1. Preparation of standing transmon-qubit state

Assume that the coupler's residual coupling strength is $\gamma_0 = 2\pi \times 0.5$ MHz. We optimize the coherent control $u(t)$ subject to the two objective functionals Eqs. (11) and (13), in which the target emitter state is specified as $|\psi_P\rangle = |1\rangle$ (i.e., $c_0 = 0$ and $c_1 = 1$) with a pulse duration of $T_0 = 10$ ns.

For comparison, we also simulate the standard Gaussian π-pulse commonly used for state flipping in ideal two-level systems, along with its DRAG correction [42] for level-leakage suppression. Figure 2(a) displays the amplitudes of these control fields. The control optimized with J_1^{ME} contains oscillating components that manage the unwanted state transitions associated with the level leakage. In contrast, the control optimized with J_1^{QSDE} exhibits a more concentrated pulse energy toward the end of the pulse. This suggests that the optimization strategy seeks to keep the emitter unexcited for as long as possible to reduce photon leakage.

Figure 2(b) illustrates the population variation of the target state $|1\rangle$ throughout the control process. At the final time $t = T_0$, the population reaches $|1\rangle$ with fidelities of 99.40% and 99.41% for the controls optimized with J_1^{ME} and J_1^{QSDE}, respectively. The DRAG pulse achieves a lower fidelity 91.56%, while the Gaussian pulse yields the poorest performance with only 82.52% fidelity.

To identify the sources of errors, in Fig. 3, we analyze the corresponding photon leakage (i.e., the total population $1 - |\xi^{(0)}|^2$ of nonvacuum field states) and the level leakage (i.e., the total population of noncomputational states $|2\rangle$, $|3\rangle$ and $|4\rangle$). In Fig. 3(a), it can be seen that the photon leakage monotonically increases with time in all cases due to the Markovian dynamics. The increase is significantly slower under the optimal controls, indicating that the photon leakage is lower compared to the Gaussian and DRAG

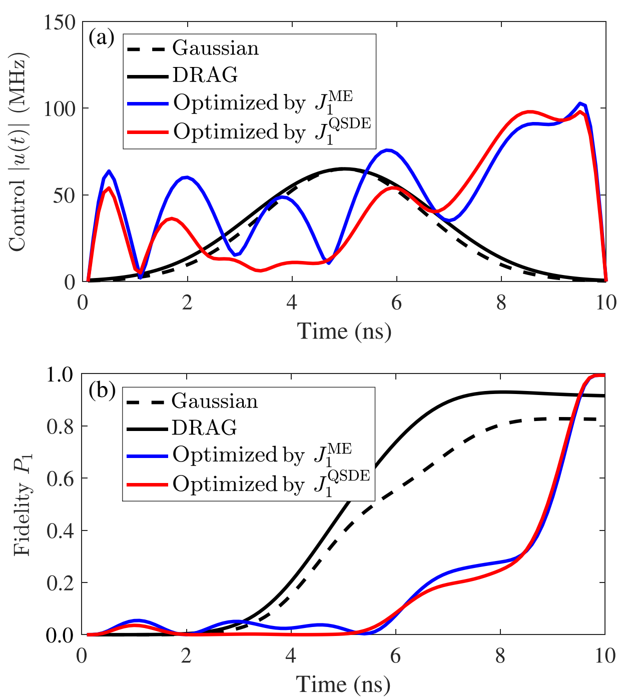

FIG. 2. (a) Amplitude of the Gaussian π-pulse, the DRAG pulse, and the optimized control pulses subject to objective functionals J_1^{ME} and J_1^{QSDE}; (b) fidelity of the transmon qubit being in the target state $|1\rangle$ during the control process.

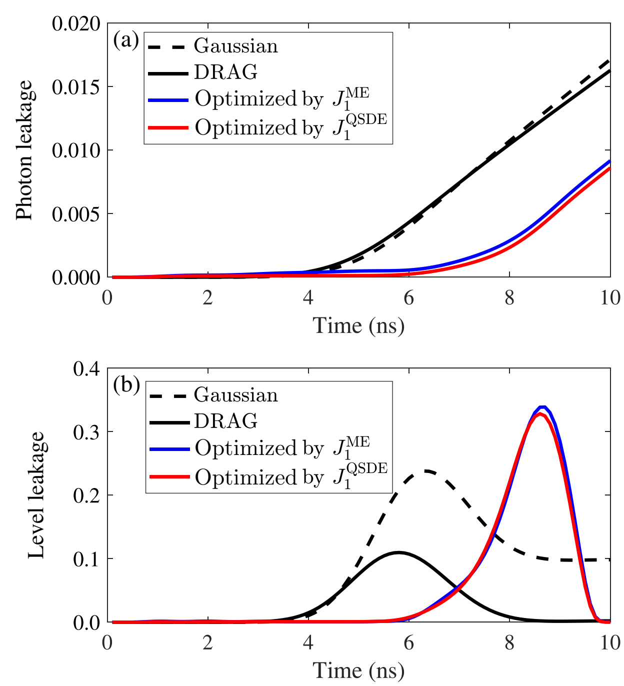

FIG. 3. (a) Photon leakage $1 - |\xi^{(0)}|^2$ and (b) level leakage (total population $P_2 + P_3 + P_4$ of noncomputational states $|2\rangle$, $|3\rangle$, and $|4\rangle$) during state preparation.

controls. Figure 3(b) demonstrates that the level leakage can be nearly completely suppressed using the DRAG pulse and the optimized pulses, while the performance of the Gaussian pulse is considerably inferior.

The error analysis provides a clear explanation for the performance differences observed in Fig. 2(b). The two optimal controls achieve high fidelities because they effectively mitigate both the photon leakage and the level leakage. Although the DRAG pulse successfully reduces errors caused by level leakage, it does not efficiently suppress the photon-leakage error, which results in population loss of $|1\rangle$ decaying to $|0\rangle$.

The simulation results are also interesting in that, although the objective functional J_1^{ME} is designed for level-leakage suppression, the resulting optimal control also effectively reduces photon leakage. Similarly, the optimal control obtained from J_1^{QSDE} can also suppress both types of leakage errors. We conjecture that the two objective functionals may be equivalent in the context of state preparation in open systems, but this remains to be confirmed in our future studies.

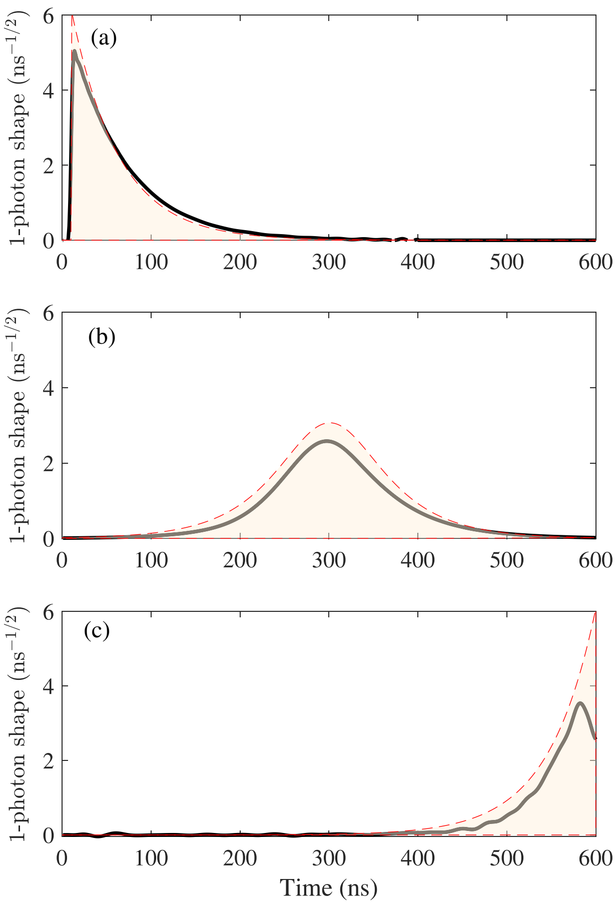

FIG. 4. Optimized shapes of single-photon components under coherent driving control and fixed coupling strength $\gamma_c = 2\pi \times 6$ MHz, where the target single-photon shapes are exponentially decaying, symmetric, and exponentially rising, respectively, with $\alpha = 2\pi \times 6$ MHz.

2. Direct generation of shaped flying qubits

Consider the direct generation of flying qubits by optimizing $u(t)$ subject to J_2 defined in Eq. (15), where the coupling strength $\gamma(t)$ is fixed at $\gamma_c = 2\pi \times 5$ MHz. The exponentially decaying, exponentially rising, and symmetric target single-photon shapes are all tested with the width parameter $\alpha = 2\pi \times 6$ MHz. The control duration is chosen as $T = 600$ ns, which is much longer than the decay time γ_c^{-1}.

In the simulations, the control pulse $u(t)$ is initiated 10 ns prior to $\xi_0(t)$ when dealing with exponentially decaying flying qubits, because the emitter must be promptly excited to $|1\rangle$ before photon emission occurs. Note that this early initiation is not required for the other two shapes, whose beginning parts rise slowly. Figure 4 displays the optimized single-photon pulse shapes, which all closely match their target waveforms. We further optimize the controls with α varying from $0.6\gamma_c$ to $1.4\gamma_c$, and in Fig. 5, we plot the relationship between the best performance (i.e., the minimal value of J_2) and the parameter α.

The simulation results indicate that the coherent control $u(t)$ possesses some capacity for single-photon shaping in the absence of a tunable coupler; however, the control performance is far from good, particularly when the target pulse shape includes a rising segment. Among the three types of shape, generating exponentially decaying flying qubits is the easiest, as this shape is similar to those produced by natural spontaneous emission. In contrast, generating flying qubits with exponentially rising shapes proves to be considerably more challenging.

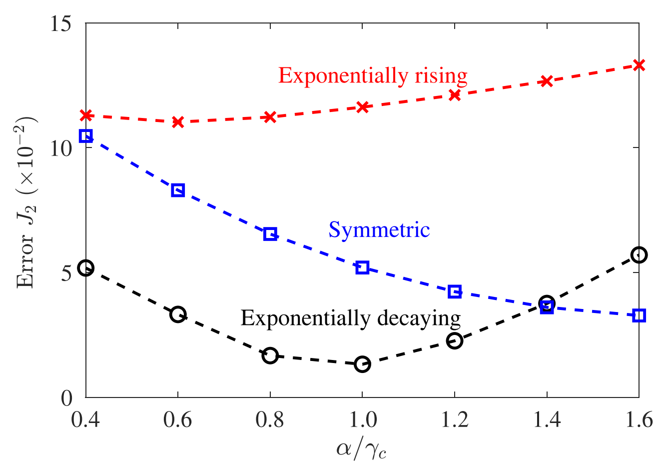

FIG. 5. Best performance achieved by coherent control for different types of single-photon shapes under different values of α ranging from $0.4\gamma_c$ to $1.6\gamma_c$.

3. State transfer from the emitter to a shaped flying qubit

We now optimize the coherent control $u(t)$ for the state transfer from the emitter to a flying qubit with exponentially decaying, exponentially rising, and symmetric shapes. The parameters are set to $\alpha = 2\pi \times 6$ MHz and $\gamma_c = 2\pi \times 5$ MHz.

The optimization is subject to J_3, as defined in Eq. (18). To assess the state-transfer performance, we plot the profiles of the single-photon components conditioned on the emitter's initial state. Ideally, a single photon $|1_{\xi_0}\rangle$ should be released [i.e., $\xi^{(1)}(t) = \xi_0(t)$] when the emitter is initiated at $|\psi_0\rangle = |1\rangle$. Conversely, when $|\psi_0\rangle = |0\rangle$, no single-photon emission is expected [i.e., $\xi^{(1)}(t) = 0$].

Figure 6 displays the conditioned single-photon components under optimal controls for the three types of target single-photon shape. Similar to the findings in Sec. IV A 3, the state transfer is almost perfect when the target single-photon shape is exponentially decaying; however, the performance is significantly poorer when the target single-photon shape is either symmetric or exponentially rising. The single-photon components conditioned on $|\psi_0\rangle = |0\rangle$ and $|\psi_0\rangle = |1\rangle$ are nearly indistinguishable, falling short of the anticipated conditional single-photon emission. The overall poor performance again indicates that the coherent control $u(t)$ offers limited capacity for single-photon shaping without a tunable coupler.

B. Flying-qubit control under tunable coupling and tunable coherent control

The above simulations collectively demonstrate the necessity of a tunable coupler for high-quality flying-qubit shaping. Next, we will demonstrate that, while coherent control is not ideal for flying-qubit shaping, it can serve as a valuable complement to enhance the performance of a tunability-limited coupler.

We begin by testing the direct generation of flying qubits with an exponentially rising shape, which is the most challenging among the three shapes. In Sec. IV A 2, the achievable minimal shaping error is 0.116 with a fixed-strength coupler ($\gamma_c = 2\pi \times 5$ MHz). On the other hand, according to Eq. (14), the shaping can be perfectly achieved without the coherent control $u(t)$ with an ideal tunable coupler as

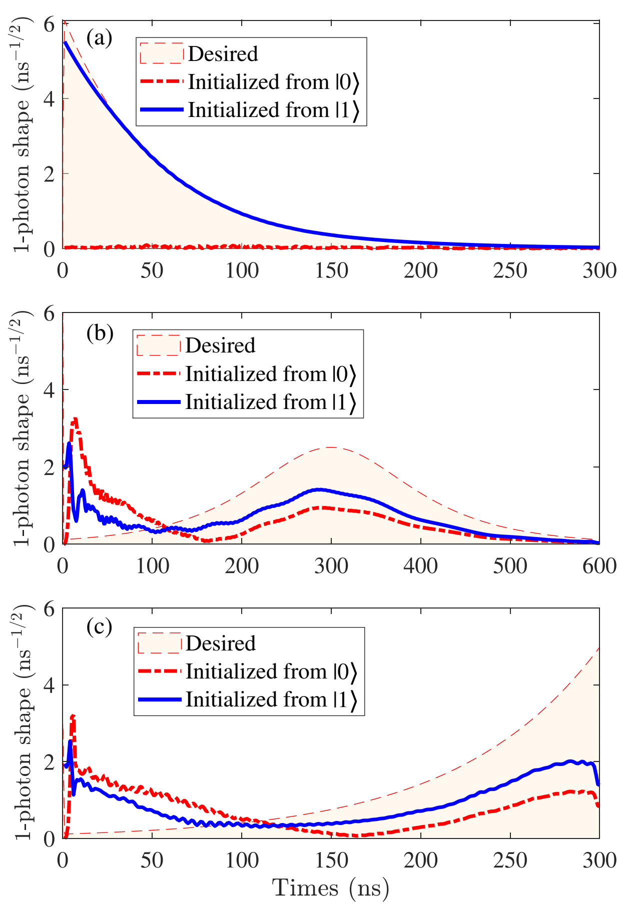

FIG. 6. Optimized state transfer from the transmon qubit to flying qubits with (a) exponentially decaying, (b) symmetric, and (c) exponentially rising photon shapes.

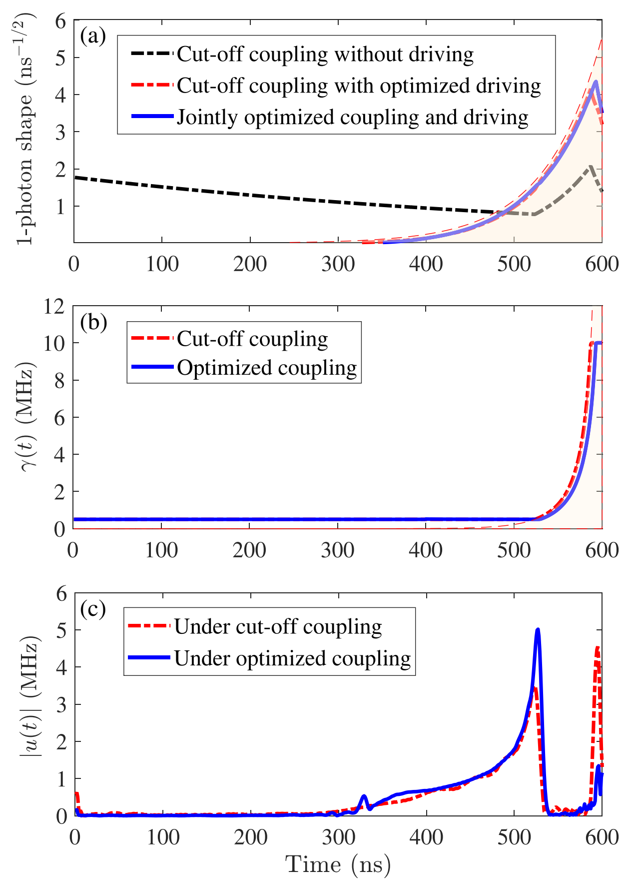

FIG. 7. Fitting result of exponentially rising shape flying qubits with the rate $\alpha = 2\pi \times 5$ MHz: (a) single-photon pulse shapes; (b) corresponding tunable coupling function; (c) amplitude of the control pulses.

follows [14]:

$$\gamma(t) = \frac{\alpha e^{\alpha(t-T)}}{1 - e^{\alpha(t-T)}}. \tag{21}$$

Nonetheless, as can be seen in Fig. 7(b), the tuning scheme (21) is unrealistic because the desired $\gamma(t)$ approaches infinity as $t \to T$.

Assume that the coupling strength of the nonideal tunable coupler is bounded below by $2\pi \times 0.5$ MHz and above by $2\pi \times 10$ MHz. An approximate tuning scheme [see Fig. 7(b)] can be derived by simply applying a cutoff to the ideal scheme described in Eq. (21). As illustrated in Fig. 7(a), the cutoff scheme produces a poorly shaped single photon, primarily due to the initial photon leakage caused by the inability to fully turn off the coupling.

We now maintain the cutoff tuning scheme and introduce the coherent control $u(t)$ as an auxiliary control. As shown in Fig. 7(a), optimizing $u(t)$ subject to J_3 allows the single-photon component to closely resemble $\xi_0(t)$, except for the final portion that requires extremely strong coupling. This optimization process reduces the control error from 0.112 to 0.038. If we allow the coupling function $\gamma(t)$ to be jointly optimized alongside $u(t)$, the control error can be further decreased from 0.038 to 0.028.

These improvements indicate that the coherent control is a useful complement to the tunability-limited coupler. As depicted in Fig. 7(c), the coherent control pulses are active in the regions where the coupler's tunability is restricted (roughly before 530 ns and after 580 ns). Within the time interval where the desired coupling strength is achievable, the coupler primarily governs the system, while the coherent control remains nearly inactive.

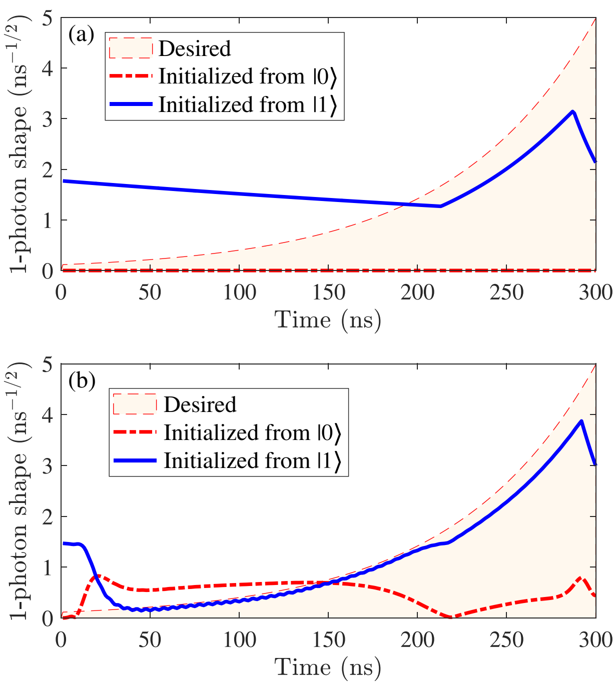

FIG. 8. Single-photon emission during the state transfer from the transmon to the flying qubit with an exponentially rising shape: (a) under cutoff coupling without coherent control; (b) under optimized coupling and optimized coherent control.

TABLE I. Error budget under state-transfer control schemes: (A) fixed coupling with tunable coherent control; (B) cutoff coupling without coherent control; (C) jointly optimized coupling and coherent control.

Control scheme	$E_{\|0\rangle\to\|\mathrm{vac}\rangle}$	$E_{\|1\rangle\to\|1_{\xi_0}\rangle}$	Total error
(A)	0.4534	0.3593	0.8127
(B)	0	0.3435	0.3435
(C)	0.0317	0.0651	0.0968

We also evaluated the optimization of state-transfer protocols using the aforementioned schemes involving a tunability-limited coupler. Simulation results are presented in Fig. 8. Compared to the coherent control scheme with a fixed coupler [see Fig. 6(c)], the cutoff coupling scheme without coherent control results in anticipated zero photon emission when the emitter's initial state is $|\psi_0\rangle = |0\rangle$, but the single-photon component conditioned on $|\psi_0\rangle = |1\rangle$ is still poorly shaped. If we jointly optimize $u(t)$ and $\gamma(t)$, the single-photon shape conditioned on $|\psi_0\rangle = |1\rangle$ is significantly improved; however, the single-photon emission conditioned on $|\psi_0\rangle = |0\rangle$ cannot be fully suppressed.

To quantitatively compare the control performances, we list in Table I the errors contributed by the conditional state-transfer infidelities for $|0\rangle \to |\mathrm{vac}\rangle$ and $|1\rangle \to |1_{\xi_0}\rangle$, respectively,

$$E_{|0\rangle\to|\mathrm{vac}\rangle} = \left|1 - \xi^{(0)}\right|^2, \tag{22}$$

$$E_{|1\rangle\to|1_{\xi_0}\rangle} = \int_0^\infty |\xi^{(1)}(t) - \xi_0(t)|^2 \, dt. \tag{23}$$

The comparisons demonstrate that the tunable coupler is more effective than coherent driving in shaping control, despite the coupler's limited tunability. Nevertheless, the coherent control plays a crucial complementary role when used in conjunction with the coupler, resulting in a significant reduction of the total error from 0.3445 to 0.0968.

V. CONCLUSION

In conclusion, we have introduced quantum optimal control theory for the manipulation of flying qubits. The proposed gradient-descent algorithm is designed for systems involving nonideal emitters and couplers. Simulation results indicate that the optimized coherent controls can effectively reduce both level and photon leakages caused by imperfections, but their shaping capabilities are constrained without a tunable coupler. Nonetheless, coherent control can serve as an important complement to enhance performance, particularly in scenarios where coupler tunability is limited.

Throughout this paper, our discussion focuses on a transmon qubit with a single input-output channel to facilitate physical comprehension. The established design framework can be seamlessly adapted to general flying-qubit control systems with more complicated emitters and multiple input-output channels. Additionally, it is compatible with various optimization methods, including Pontryagin's minimum principle [43] and the Krotov method [44]. In the presence of other nonidealities such as parametric uncertainties and pulse distortions in the control lines [45], control fidelities can be further improved through robust quantum control [46] or reinforcement learning techniques [47].

This study paves the way for a range of intriguing problems in flying-qubit control, such as the generation of entangled or correlated flying qubits for quantum information distribution, as well as the capture and conversion of flying qubits. Additionally, the established framework can be used to design flying-qubit-mediated remote quantum gates between distant stationary qubits. These topics will be explored in our future studies.

ACKNOWLEDGMENTS

This work is supported by the Innovation Program for Quantum Science and Technology (Grants No. 2021ZD0300200, 2021ZD0301800, and 2023ZD0300600), NSFC (Grants No. 62173201, 62173288, and 92365209), Guangdong Provincial Quantum Science Strategic Initiative (Grant No. GDZX2200001), and Hong Kong Research Grant Council (RGC) (Grant No. 15213924).

DATA AVAILABILITY

The data that support the findings of this study are available from the corresponding author.

APPENDIX A: GRADIENT VECTOR FORMULAS

The calculation of gradient vectors is the key part of the optimization algorithm. Here, we present the gradient-vector formulas for the proposed objective functionals J_1^{QSDE}, J_2, and J_3, which all rely on the evolution equation (5). The gradient vector of J_1^{ME} can be found in the literature (e.g., using QUTIP [48]) and will not be discussed here.

To numerically evaluate the objective functionals and their gradients, we choose a sufficiently long time interval $[0, T]$ so that the field emitted after $t = T$ is negligible. The time interval is then evenly discretized into M pieces with $\Delta t = T/M$. Denote $t_k = k\Delta t$, $k = 0, 1, \ldots, M$, and assume that both $u(t)$ and $\gamma(t)$ are piecewise-constant functions over subintervals $[t_{k-1}, t_k]$, $k = 1, \ldots, M$. The transition operator from t_j to t_n can be calculated as

$$G_{n,j} \triangleq G(t_n, t_j) = V_n \cdots V_{j+2} V_{j+1}, \tag{A1}$$

where $V_k = e^{-iH_{\text{eff}}(t_k)\Delta t}$.

According to the first-order perturbation, we have

$$\Delta V_j \approx \Big[-i\Delta u_x(t_j)(\hat{a}^\dagger + \hat{a}) + \Delta u_y(t_j)(\hat{a}^\dagger - \hat{a}) - \frac{\Delta\gamma(t_j)}{2}\hat{a}^\dagger\hat{a}\Big] V_j \Delta t, \tag{A2}$$

which leads to the elementary partial derivatives

$$\frac{\partial V_k}{\partial u_x(t_j)} \approx -i\delta_{jk}(\hat{a}^\dagger + \hat{a}) V_k \Delta t, \tag{A3}$$

$$\frac{\partial V_k}{\partial u_y(t_j)} \approx \delta_{jk}(\hat{a}^\dagger - \hat{a}) V_k \Delta t, \tag{A4}$$

$$\frac{\partial V_k}{\partial \gamma(t_j)} \approx -\delta_{jk}\frac{\hat{a}^\dagger\hat{a}}{2} V_k \Delta t, \tag{A5}$$

where δ_{jk} is the Kronecker symbol.

Based on Eqs. (A3)–(A5), it is straightforward to derive the following:

$$\frac{\partial J_1^{\text{QSDE}}}{\partial u_x(t_j)} \approx 2\text{Re}\left\{ i\langle\psi_P|G_{M_0,j}\left(\hat{a}^\dagger + \hat{a}\right) G_{j,0}|0\rangle \Delta t \left(\langle\psi_P|G_{M_0,0}|0\rangle\right)^* \right\} \tag{A6}$$

$$\frac{\partial J_1^{\text{QSDE}}}{\partial u_y(t_j)} \approx -2\text{Re}\left\{ \langle\psi_P|G_{M_0,j}\left(\hat{a}^\dagger - \hat{a}\right) G_{j,0}|0\rangle \Delta t \left(\langle\psi_P|G_{M_0,0}|0\rangle\right)^* \right\} \tag{A7}$$

where $j = 1, \ldots, M_0$ with $M_0 = T_0/\Delta t$.

The calculation of gradient vectors for J_2 and J_3 is more complicated. Taking J_3 as an example, we can first approximate it as the following summation:

$$J_3 \approx |\xi^{(0)} - 1|^2 + \sum_{n=1}^{M} \left|\xi^{(1)}(t_n) - \xi_0(t_n)\right|^2 \Delta t, \tag{A8}$$

from which the gradient vector can be calculated as follows:

$$\frac{\partial J_3}{\partial \mathbf{c}(t_j)} \approx 2\text{Re}\left\{ \frac{\partial \xi^{(0)}}{\partial \mathbf{c}(t_j)}(\xi^{(0)} - 1)^* + \sum_{n=1}^{M} \frac{\partial \xi^{(1)}(t_n)}{\partial \mathbf{c}(t_j)} \left[\xi^{(1)}(t_n) - \xi_0(t_n)\right]^* \Delta t \right\}, \tag{A9}$$

where $\mathbf{c}(t) \in \{u_x(t), u_y(t), \gamma(t)\}$.

Thus, it is sufficient to compute the derivatives of $\xi^{(0)}$ and $\xi^{(1)}(t)$ with respect to the control variables. Applying the elementary derivatives (A3)–(A5), it is not hard to obtain

$$\frac{\partial \xi^{(0)}}{\partial u_x(t_j)} \approx -i\langle 0|G_{M,j}\left(\hat{a}^\dagger + \hat{a}\right)G_{j,0}|0\rangle\Delta t, \tag{A10}$$

$$\frac{\partial \xi^{(0)}}{\partial u_y(t_j)} \approx \langle 0|G_{M,j}\left(\hat{a}^\dagger - \hat{a}\right)G_{j,0}|0\rangle\Delta t, \tag{A11}$$

$$\frac{\partial \xi^{(0)}}{\partial \gamma(t_j)} \approx -\frac{1}{2}\langle 0|G_{M,j}\hat{a}^\dagger\hat{a}G_{j,0}|0\rangle\Delta t. \tag{A12}$$

and

$$\frac{\partial \xi^{(1)}(t_n)}{\partial u_x(t_j)} \approx \begin{cases} -i\sqrt{\gamma(t_n)}\langle 0|G_{M,n}\hat{a}G_{n,j}\left(\hat{a}^\dagger + \hat{a}\right)G_{j,0}|1\rangle\Delta t, & t_j \leqslant t_n, \\ -i\sqrt{\gamma(t_n)}\langle 0|G_{M,j}\left(\hat{a}^\dagger + \hat{a}\right)G_{j,n}\hat{a}G_{n,0}|1\rangle\Delta t, & t_j > t_n. \end{cases} \tag{A13}$$

$$\frac{\partial \xi^{(1)}(t_n)}{\partial u_y(t_j)} \approx \begin{cases} \sqrt{\gamma(t_n)}\langle 0|G_{M,n}\hat{a}G_{n,j}\left(\hat{a}^\dagger - \hat{a}\right)G_{j,0}|1\rangle\Delta t, & t_j \leqslant t_n, \\ \sqrt{\gamma(t_n)}\langle 0|G_{M,j}\left(\hat{a}^\dagger - \hat{a}\right)G_{j,n}\hat{a}G_{n,0}|1\rangle\Delta t, & t_j > t_n. \end{cases} \tag{A14}$$

$$\frac{\partial \xi^{(1)}(t_n)}{\partial \gamma(t_j)} \approx \begin{cases} -\frac{\sqrt{\gamma(t_n)}}{2}\langle 0|G_{M,n}\hat{a}G_{n,j}\hat{a}^\dagger\hat{a}G_{j,0}|\psi_0\rangle\Delta t, & t_j < t_n, \\ -\frac{\sqrt{\gamma(t_n)}}{2}\langle 0|G_{M,j}\hat{a}\left[\hat{a}^\dagger\hat{a} - \gamma^{-1}(t_j)\right]G_{j,0}|1\rangle\Delta t, & t_j = t_n, \\ -\frac{\sqrt{\gamma(t_n)}}{2}\langle 0|G_{M,j}\hat{a}^\dagger\hat{a}G_{j,n}\hat{a}G_{n,0}|1\rangle\Delta t, & t_j > t_n. \end{cases} \tag{A15}$$

The gradient-vector calculation of J_3 defined by Eq. (15) is very similar to that of J_2 described above, and the corresponding formulas will not be provided here.

In the simulations, we incorporate practical constraints on the coherent control variables. Let $\vec{u}_{x,y} = [u_{x,y}(t_0, \ldots, t_M)]$ be the vectors of variables to be optimized. We begin by selecting a smooth envelope function $s(t)$ with $s(t_0) = s(t_M) = 0$ and a linear low-pass filter that can be represented by a matrix F_{LP} acting on $\vec{u}_{x,y}$. We choose control vectors in the following form:

$$\vec{u}_{x,y} = S_{\mathrm{en}}F_{\mathrm{LP}}\vec{v}_{x,y},$$

where $\vec{v}_{x,y}$ is unconstrained and

$$S_{\mathrm{en}} = \mathrm{diag}\{s(t_0), \ldots, s(t_M)\}.$$

By this means, the control amplitudes always start and end at zero values and are smoothed out during the optimization.

The corresponding optimization problem can be easily transformed into an unconstrained problem with respect to $\vec{v}_{x,y}$. The gradient vector can be computed as follows:

$$\frac{\partial J}{\partial \vec{v}_{x,y}} = (S_{\mathrm{en}}F_{\mathrm{LP}})^\top \frac{\partial J}{\partial \vec{u}_{x,y}},$$

where $\partial J/\partial \vec{u}_{x,y}$ can be calculated from the above derivations.

We also impose a bound B on the control amplitudes. Accordingly, the gradient formulas remain unchanged when $|u_{x,y}(t_j)| < B$. When the bound is saturated, we need to set $\partial J/\partial u_{x,y}(t_j) = 0$.

[1] T. D. Ladd, F. Jelezko, R. Laflamme, Y. Nakamura, C. Monroe, and J. L. O'Brien, Quantum computers, Nature **464**, 45 (2010).

[2] S.-H. Wei, B. Jing, X.-Y. Zhang, J.-Y. Liao, C.-Z. Yuan, B.-Y. Fan, C. Lyu, D.-L. Zhou, Y. Wang, G.-W. Deng, H.-Z. Song, D. Oblak, G.-C. Guo, and Q. Zhou, Towards real-world quantum networks: A review, Laser Photonics Rev. **16**, 2100219 (2022).

[3] D. P. DiVincenzo, Quantum computation, Science **270**, 255 (1995).

[4] J. I. Cirac, P. Zoller, H. J. Kimble, and H. Mabuchi, Quantum state transfer and entanglement distribution among distant nodes in a quantum network, Phys. Rev. Lett. **78**, 3221 (1997).

[5] A. A. Houck, D. Schuster, J. Gambetta, J. Schreier, B. Johnson, J. Chow, L. Frunzio, J. Majer, M. Devoret, S. Girvin, *et al.*, Generating single microwave photons in a circuit, Nature **449**, 328 (2007).

[6] A. N. Korotkov, Flying microwave qubits with nearly perfect transfer efficiency, Phys. Rev. B **84**, 014510 (2011).

[7] É. Dumur, K. Satzinger, G. Peairs, M.-H. Chou, A. Bienfait, H.-S. Chang, C. Conner, J. Grebel, R. Povey, Y. Zhong, *et al.*, Quantum communication with itinerant surface acoustic wave phonons, npj Quantum Inf. **7**, 173 (2021).

[8] M. Yamamoto, S. Takada, C. Bäuerle, K. Watanabe, A. D. Wieck, and S. Tarucha, Electrical control of a solid-state flying qubit, Nat. Nanotechnol. **7**, 247 (2012).

[9] M. Mirhosseini, A. Sipahigil, M. Kalaee, and O. Painter, Superconducting qubit to optical photon transduction, Nature **588**, 599 (2020).

[10] J. Ilves, S. Kono, Y. Sunada, S. Yamazaki, M. Kim, K. Koshino, and Y. Nakamura, On-demand generation and characterization of a microwave time-bin qubit, npj Quantum Inf. **6**, 34 (2020).

[11] X. Gu, A. F. Kockum, A. Miranowicz, Y.-X. Liu, and F. Nori, Microwave photonics with superconducting quantum circuits, Phys. Rep. **718**, 1 (2017).

[12] M. Pechal, L. Huthmacher, C. Eichler, S. Zeytinoglu, A. A. Abdumalikov, S. Berger, A. Wallraff, and S. Filipp, Microwave-controlled generation of shaped single photons in circuit quantum electrodynamics, Phys. Rev. X **4**, 041010 (2014).

[13] P. Forn-Diaz, C. Warren, C. Chang, A. Vadiraj, and C. Wilson, On-demand microwave generator of shaped single photons, Phys. Rev. Appl. **8**, 054015 (2017).

[14] W.-L. Li, G. Zhang, and R.-B. Wu, On the control of flying qubits, Automatica **143**, 110338 (2022).

[15] M. Pierre, I.-M. Svensson, S. Raman Sathyamoorthy, G. Johansson, and P. Delsing, Storage and on-demand release of microwaves using superconducting resonators with tunable coupling, Appl. Phys. Lett. **104**, 232604 (2014).

[16] Y. Yin, Y. Chen, D. Sank, P. OMalley, T. White, R. Barends, J. Kelly, E. Lucero, M. Mariantoni, A. Megrant, *et al.*, Catch and release of microwave photon states, Phys. Rev. Lett. **110**, 107001 (2013).

[17] I.-C. Hoi, C. Wilson, G. Johansson, T. Palomaki, B. Peropadre, and P. Delsing, Demonstration of a single-photon router in the microwave regime, Phys. Rev. Lett. **107**, 073601 (2011).

[18] I.-C. Hoi, T. Palomaki, J. Lindkvist, G. Johansson, P. Delsing, and C. Wilson, Generation of nonclassical microwave states using an artificial atom in 1D open space, Phys. Rev. Lett. **108**, 263601 (2012).

[19] Y. Zhong, H.-S. Chang, K. Satzinger, M.-H. Chou, A. Bienfait, C. Conner, É. Dumur, J. Grebel, G. Peairs, R. Povey, *et al.*, Violating Bell's inequality with remotely connected superconducting qubits, Nat. Phys. **15**, 741 (2019).

[20] Y. Zhong, H.-S. Chang, A. Bienfait, É. Dumur, M.-H. Chou, C. R. Conner, J. Grebel, R. G. Povey, H. Yan, D. I. Schuster, *et al.*, Deterministic multi-qubit entanglement in a quantum network, Nature **590**, 571 (2021).

[21] Z. Peng, S. De Graaf, J. Tsai, and O. Astafiev, Tuneable on-demand single-photon source in the microwave range, Nat. Commun. **7**, 12588 (2016).

[22] Y. Zhou, Z. Peng, Y. Horiuchi, O. Astafiev, and J. Tsai, Tunable microwave single-photon source based on transmon qubit with high efficiency, Phys. Rev. Appl. **13**, 034007 (2020).

[23] W. Yao, R. Liu, and L. J. Sham, Theory of control of the spin-photon interface for quantum networks, Phys. Rev. Lett. **95**, 030504 (2005).

[24] H. I. Nurdin, M. R. James, and N. Yamamoto, in *2016 IEEE 55th IEEE Conference on Decision and Control (CDC) (Las Vegas, NV, USA, 2016), pp. 2513–2518.*

[25] W. Li, X. Dong, G. Zhang, and R.-B. Wu, Flying-qubit control via a three-level atom with tunable waveguide couplings, Phys. Rev. B **106**, 134305 (2022).

[26] J. Qiu, Y. Liu, J. Niu, L. Hu, Y. Wu, L. Zhang, W. Huang, Y. Chen, J. Li, S. Liu, Y. Zhong, L. Duan, and D. Yu, Deterministic quantum teleportation between distant superconducting chips, Sci. Bull. **70**, 351 (2025).

[27] B. Kannan, A. Almanakly, Y. Sung, A. Di Paolo, D. A. Rower, J. Braumüller, A. Melville, B. M. Niedzielski, A. Karamlou, K. Serniak, *et al.*, On-demand directional microwave photon emission using waveguide quantum electrodynamics, Nat. Phys. **19**, 394 (2023).

[28] Y. Chen, C. Neill, P. Roushan, N. Leung, M. Fang, R. Barends, J. Kelly, B. Campbell, Z. Chen, B. Chiaro, *et al.*, Qubit architecture with high coherence and fast tunable coupling, Phys. Rev. Lett. **113**, 220502 (2014).

[29] F. Yan, P. Krantz, Y. Sung, M. Kjaergaard, D. L. Campbell, T. P. Orlando, S. Gustavsson, and W. D. Oliver, Tunable coupling scheme for implementing high-fidelity two-qubit gates, Phys. Rev. Appl. **10**, 054062 (2018).

[30] P. Kurpiers, P. Magnard, T. Walter, B. Royer, M. Pechal, J. Heinsoo, Y. Salathé, A. Akin, S. Storz, J.-C. Besse, *et al.*, Deterministic quantum state transfer and remote entanglement using microwave photons, Nature **558**, 264 (2018).

[31] E. A. Sete, A. Q. Chen, R. Manenti, S. Kulshreshtha, and S. Poletto, Floating tunable coupler for scalable quantum computing architectures, Phys. Rev. Appl. **15**, 064063 (2021).

[32] N. Khaneja, T. Reiss, C. Kehlet, T. Schulte-Herbrüggen, and S. J. Glaser, Optimal control of coupled spin dynamics: Design of NMR pulse sequences by gradient ascent algorithms, J. Magn. Reson. **172**, 296 (2005).

[33] D. M. Reich, M. Ndong, and C. P. Koch, Monotonically convergent optimization in quantum control using Krotov's method, J. Chem. Phys. **136**, 104103 (2012).

[34] U. Boscain, M. Sigalotti, and D. Sugny, Introduction to the Pontryagin maximum principle for quantum optimal control, PRX Quantum **2**, 030203 (2021).

[35] G. Zhang and M. R. James, On the response of quantum linear systems to single photon input fields, IEEE Trans. Autom. Control **58**, 1221 (2013).

[36] R. Loudon, *The Quantum Theory of Light* (OUP Oxford, Oxford, 2000).

[37] K. Fischer, R. Trivedi, V. Ramasesh, I. Siddiqi, and J. Vučković, Scattering into one-dimensional waveguides from a coherently-driven quantum-optical system, Quantum **2**, 69 (2018).

[38] R. Trivedi, K. Fischer, S. Xu, S. Fan, and J. Vuckovic, Few-photon scattering and emission from low-dimensional quantum systems, Phys. Rev. B **98**, 144112 (2018).

[39] G. Lindblad, On the generators of quantum dynamical semigroups, Commun. Math. Phys. **48**, 119 (1976).

[40] H.-P. Breuer and F. Petruccione, *The Theory of Open Quantum Systems* (Oxford University Press, USA, 2002).

[41] J. E. Dennis, Jr. and J. J. Moré, Quasi-Newton methods, motivation and theory, SIAM Rev. **19**, 46 (1977).

[42] F. Motzoi, J. M. Gambetta, P. Rebentrost, and F. K. Wilhelm, Simple pulses for elimination of leakage in weakly nonlinear qubits, Phys. Rev. Lett. **103**, 110501 (2009).

[43] S. Bao, S. Kleer, R. Wang, and A. Rahmani, Optimal control of superconducting gmon qubits using Pontryagin's minimum principle: Preparing a maximally entangled state with singular bang-bang protocols, Phys. Rev. A **97**, 062343 (2018).

[44] D. J. Tannor, V. Kazakov, and V. Orlov, in *Proceedings of the NATO Advanced Research Workshop*, Edited by J. Broeckhove and L. Lathouwers, NATO ASI B (Plenum Press, New York, 1992), Vol. 299, pp. 347–360.

[45] X. Cao, B. Chu, Y.-X. Liu, Z. Peng, and R.-B. Wu, Learning to calibrate quantum control pulses by iterative deconvolution, IEEE Trans. Control Syst. Technol. **30**, 193 (2022).

[46] R.-B. Wu, H. Ding, D. Dong, and X. Wang, Learning robust and high-precision quantum controls, Phys. Rev. A **99**, 042327 (2019).

[47] V. V. Sivak, A. Eickbusch, H. Liu, B. Royer, I. Tsioutsios, and M. H. Devoret, Model-free quantum control with reinforcement learning, Phys. Rev. X **12**, 011059 (2022).

[48] J. R. Johansson, P. D. Nation, and F. Nori, QuTiP: An open-source Python framework for the dynamics of open quantum systems, Comput. Phys. Commun. **183**, 1760 (2012).